Formation of vacancies and copper substitutionals in potassium sodium niobate under various processing conditions

Sabine Körbel,* Pavel Marton, and Christian Elsässer
Fraunhofer Institute for Mechanics of Materials IWM, Wöhlerstraße 11, 79108 Freiburg, Germany
(Received 26 January 2010; revised manuscript received 22 April 2010; published 21 May 2010)

In the lead-free perovskite potassium sodium niobate, the thermodynamically preferred lattice sites and charge states of vacancies and substitutional Cu atoms for different processing conditions are determined theoretically from first principles. For that purpose, defect-formation energies of vacancies and Cu substitutionals in different charge states are calculated with the density-functional theory in the local-density approximation using norm-conserving pseudopotentials and a mixed-basis supercell approach. The formation energy of vacancies and the relative stability of Cu substitutionals on alkali and Nb sites in potassium sodium niobate are determined for oxygen-rich and oxygen-poor processing conditions and as function of the Fermi energy, and the densities of states are analyzed in terms of free charge carriers.

DOI: 10.1103/PhysRevB.81.174115 PACS number(s): 61.72.Bb, 61.72.U−, 71.15.Mb, 77.84.Ek

I. INTRODUCTION

The lead-free ferroelectric ceramic potassium sodium niobate $(K,Na)NbO_3$ (KNN) is a nontoxic possible future alternative to the widely used lead zirconate titanate $Pb(Zr,Ti)O_3$ (PZT) for the electroactive component in piezoelectric actuators and sensors.[1] $KNbO_3$ (KNO) and $NaNbO_3$ (NNO) can form solid solution compounds over the whole composition range from KNO to NNO. Near a composition of K:Na =50:50 a morphotropic phase boundary, which is analogous to that in PZT with Zr:Ti≈50:50, leads to enhanced ferroelectric properties, which is a major reason why KNN is regarded as a promising lead-free substitute for PZT.

KNN ceramics are produced for instance via an alkali carbonate and niobium oxide processing technology.[2] Dopant elements can be added by mixing their oxides with the host constituents before calcination and sintering. Adding copper oxide as a sintering aid was found to improve the densification of the ceramic KNN,[1,3] possibly by forming a liquid phase, which can act as a vehicle for atom transport and therefore facilitate grain growth.[4,5] Besides this processing aspect, Cu doping in alkali niobates also affects their electronic and ferroelectric properties. In Ref. 6 it is assumed that Cu atoms substitute Nb atoms (on *B* sites in the perovskite structure ABO_3), and oxygen vacancies are formed as a charge compensation mechanism. In Ref. 7 Cu is suggested to substitute both alkali and Nb atoms (on *A* or *B* sites, respectively). While Cu^{2+} on a Nb^{5+} site can act as an acceptor dopant and lead to ferroelectric hardening, it could act as a donor on a Na^+ or K^+ site and cause ferroelectric softening. In this work, in order to investigate the site preference for Cu dopants and the prevailing vacancy type as function of the chemical processing conditions, first-principles density-functional-theory (DFT) calculations were carried out to determine the thermodynamic stability conditions for defect configurations and charge states of vacancies and substitutional Cu impurities in KNN.

The defect-formation enthalpy, which determines the preferred lattice site for the dopant, depends on the chemical potentials of the atomic reservoirs,[8] which for gases (oxygen in the case of KNN) correspond to the chemical conditions in terms of partial pressures of the elemental constituents during processing.[9] In the present work the influence of the processing conditions is investigated systematically according to the thermodynamic first-principles formalism outlined in, e.g., Ref. 10.

First-principles calculations have already been applied to various ferroelectric materials by many authors, e.g., copper and iron doping in lead titanate,[11] vacancies in alkali niobates,[12,13] and iron impurities in potassium niobate[14] have been investigated. But to our knowledge no such studies of Cu doping of alkali niobates have been reported so far and comparable published studies of vacancies in the KNN system have been limited to neutral vacancies.

II. THERMODYNAMIC FORMALISM

The preferred lattice site for a dopant is governed by the defect-formation enthalpy, which for most cases of inorganic solid state systems can be approximated by the defect-formation energy.[8] The defect-formation energy E^f for a defect X in a charge state q is given by[8]

$$E^f[X^q] = E_{\mathrm{tot}}[X^q] - E_{\mathrm{tot}}[\mathrm{bulk}] - \sum_i \mu_i n_i + q(E_F + E_{\mathrm{VBM}} + \Delta V), \quad (1)$$

where $E_{\mathrm{tot}}[X^q]$ is the total energy of the supercell containing a defect X with charge q and $E_{\mathrm{tot}}[\mathrm{bulk}]$ is the total energy of a perfect cell of the same size. μ_i is the chemical potential of atom species i, n_i is the number of atoms of species i that is exchanged with a reservoir in the defect formation reaction ($n_i>0$ for species that are added to, $n_i<0$ for species that are removed from the host crystal), and E_F is the Fermi energy, i.e., the chemical potential of an electron relative to the energy of the valence-band maximum (VBM), E_{VBM}, and ΔV is a correction term which aligns the energy zero of the material with a defect to that of the perfect material.[8] For charged defects, $-q$ is the number of excess electrons assigned to the defect. We corrected the total energies of defective cells by the number of electrons in the conduction band multiplied with the difference between local-density

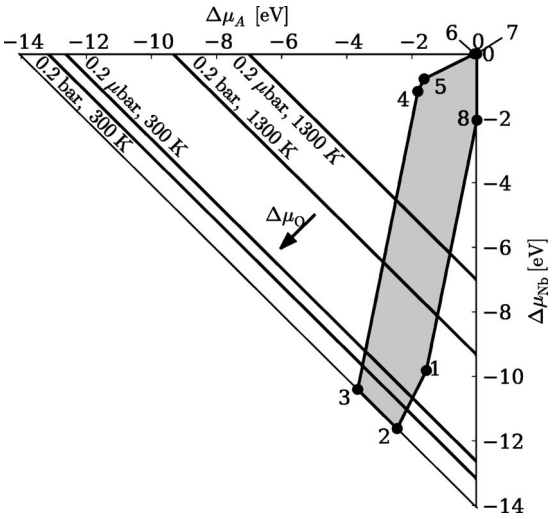

FIG. 1. Region of possible values for the relative chemical potentials as defined in Eq. (2). The area inside the outer triangle is given by the Eqs. (3) and (4), the shaded area remains after taking into account the Eqs. (5). The diagonal lines indicate the chemical potentials of oxygen that correspond to oxygen partial pressures in air at the standard atmospheric pressure and in air at 10^{-6} bar, for the temperatures 300 and 1300 K.

approximation (LDA) band gap and the experimental one (see also Sec. III). Assuming chemical equilibrium conditions, the chemical potentials of the constituents can vary in ranges that are given by requiring the perovskite phase to be stable and the fact that the chemical potentials cannot exceed those of the composing elements in their most stable phases (see Table III for the relevant numerical values).

In the following, relative chemical potentials $\Delta\mu_i$ are used:

$$\Delta\mu_i = \mu_i - \mu_i^0, \tag{2}$$

where μ_i^0 is the chemical potential of species i in its most stable elemental phase. In equilibrium, the alkali niobate perovskite $A\mathrm{NbO_3}$ is stable if

$$\Delta\mu_A + \Delta\mu_{\mathrm{Nb}} + 3\Delta\mu_{\mathrm{O}} = \Delta H_f^0(A\mathrm{NbO_3}), \tag{3}$$

where $\Delta H_f^0(A\mathrm{NbO_3})$ is the formation enthalpy of $A\mathrm{NbO_3}$ from its elemental constituents.

The upper boundary for the chemical potentials is

$$\Delta\mu_i \leq 0 \tag{4}$$

since otherwise the elemental phase of component i would precipitate.

The outer triangle in Fig. 1 shows the allowed range of the chemical potentials for the alkali (A) and Nb atoms according to Eqs. (3) and (4). The allowed region is further confined by the competing oxide phases $A_2\mathrm{O}$, $A_2\mathrm{O_2}$, NbO, $\mathrm{NbO_2}$, and $\mathrm{Nb_2O_5}$:

$$2\Delta\mu_A + \Delta\mu_{\mathrm{O}} \leq \Delta H_f^0(A_2\mathrm{O}),$$

$$2\Delta\mu_A + 2\Delta\mu_{\mathrm{O}} \leq \Delta H_f^0(A_2\mathrm{O_2}),$$

$$\Delta\mu_{\mathrm{Nb}} + \Delta\mu_{\mathrm{O}} \leq \Delta H_f^0(\mathrm{NbO}),$$

$$\Delta\mu_{\mathrm{Nb}} + 2\Delta\mu_{\mathrm{O}} \leq \Delta H_f^0(\mathrm{NbO_2}),$$

$$2\Delta\mu_{\mathrm{Nb}} + 5\Delta\mu_{\mathrm{O}} \leq \Delta H_f^0(\mathrm{Nb_2O_5}). \tag{5}$$

In our case of a mixed perovskite, where the A sites are occupied partly by K and partly by Na atoms, the two A species introduce an additional degree of freedom. However, because metallic Na and K crystallize in the same structure, and the formation enthalpies for the two alkali metals and their oxides are of similar magnitude, in the calculation of the chemical potentials we assumed $\Delta\mu_{\mathrm{K}} = \Delta\mu_{\mathrm{Na}} = \Delta\mu_A$ and set

$$\Delta H_f^0(\text{bcc } A) = \frac{1}{2}[\Delta H_f^0(\text{bcc K}) + \Delta H_f^0(\text{bcc Na})],$$

$$\Delta H_f^0(A_2\mathrm{O}) = \frac{1}{2}[\Delta H_f^0(\mathrm{K_2O}) + \Delta H_f^0(\mathrm{Na_2O})],$$

$$\Delta H_f^0(A_2\mathrm{O_2}) = \frac{1}{2}[\Delta H_f^0(\mathrm{K_2O_2}) + \Delta H_f^0(\mathrm{Na_2O_2})]. \tag{6}$$

The ranges of the chemical potentials that remain after taking into account Eqs. (5) are indicated by the gray area in Fig. 1.

Different processing conditions correspond to different combinations of the chemical potentials. The points indicated by the numbers 1–8 in Fig. 1 cover all extremes of the possible conditions. These extremes correspond to the equality in two of the Eqs. (4) and (5). For each of the points 1–8, the $A\mathrm{NbO_3}$ perovskite and two reservoir materials are in thermodynamical equilibrium. For instance, at point 2, $A\mathrm{NbO_3}$, $\mathrm{O_2}$, and $A_2\mathrm{O_2}$ are in equilibrium. Together with Eq. (3), which must hold for all points, three equations for each point determine the three chemical potentials of A, Nb, and O:

Point 1

$$2\Delta\mu_A + \Delta\mu_{\mathrm{O}} = \Delta H_f^0(A_2\mathrm{O}),$$

$$2\Delta\mu_A + 2\Delta\mu_{\mathrm{O}} = \Delta H_f^0(A_2\mathrm{O_2}).$$

Point 2

$$\Delta\mu_{\mathrm{O}} = 0,$$

$$2\Delta\mu_A + 2\Delta\mu_{\mathrm{O}} = \Delta H_f^0(A_2\mathrm{O_2}).$$

Point 3

$$\Delta\mu_{\mathrm{O}} = 0,$$

$$2\Delta\mu_{\mathrm{Nb}} + 5\Delta\mu_{\mathrm{O}} = \Delta H_f^0(\mathrm{Nb_2O_5}).$$

Point 4

$$2\Delta\mu_{\mathrm{Nb}} + 5\Delta\mu_{\mathrm{O}} = \Delta H_f^0(\mathrm{Nb_2O_5}),$$

$$\Delta\mu_{\mathrm{Nb}} + 2\Delta\mu_{\mathrm{O}} = \Delta H_f^0(\mathrm{NbO_2}).$$

Point 5

TABLE I. Relative chemical potential of oxygen, $\Delta\mu_O$, in eV for oxygen partial pressures of 0.2 bar and 0.2 μbar, for the temperatures 300 and 1300 K, respectively.

300 K		1300 K	
0.2 bar	0.2 μbar	0.2 bar	0.2 μbar
−0.295	−0.473	−1.576	−2.350

$$\Delta\mu_{Nb} + 2\Delta\mu_O = \Delta H_f^0(NbO_2),$$

$$\Delta\mu_{Nb} + \Delta\mu_O = \Delta H_f^0(NbO).$$

Point 6

$$\Delta\mu_{Nb} = 0,$$

$$\Delta\mu_{Nb} + \Delta\mu_O = \Delta H_f^0(NbO).$$

Point 7

$$\Delta\mu_{Nb} = 0,$$

$$\Delta\mu_A = 0.$$

Point 8

$$\Delta\mu_A = 0,$$

$$2\Delta\mu_A + \Delta\mu_O = \Delta H_f^0(A_2O).$$

The chemical potential of oxygen can be related to the oxygen partial pressure and the temperature via the ideal gas equation[9]

$$\begin{aligned}\mu_O(T,p) &= \frac{1}{2}G_{O_2}(T,p)\\ &= \frac{1}{2}[H_{O_2}(T,p_0) - TS_{O_2}(T,p_0)] + \frac{1}{2}k_BT\ln\left(\frac{p}{p_0}\right)\\ &= \mu_O(T,p_0) + \frac{1}{2}k_BT\ln\left(\frac{p}{p_0}\right),\end{aligned} \quad (7)$$

where p_0 is a reference oxygen partial pressure (the standard atmospheric pressure, about 1 bar), T is the temperature, G is the Gibbs free energy per molecule, and H and S are enthalpy and entropy per oxygen molecule, which can be found in thermochemical tables and were taken from Ref. 15. For a derivation of Eq. (7) see e.g., Ref. 9. We calculated the oxygen chemical potentials (cf. Table I) that correspond to air at the standard atmospheric pressure ($p_{O_2} \approx 0.2$ bar) and to air at 1 μbar ($p_{O_2} \approx 0.2$ μbar), indicated by diagonal lines in Fig. 1, at about room temperature (300 K) and at 1300 K, the latter being in the range of typical sintering temperatures for KNN.[2]

III. COMPUTATIONAL METHOD

DFT in the LDA was employed to determine defect-formation energies of Na, K, Nb, and O vacancies and substitutional Cu atoms in $K_{0.5}Na_{0.5}NbO_3$. The defect-formation energies were calculated for atomistic supercell models containing $2\times2\times2$ fcc unit cells (80 atoms). Some results obtained with $2\times2\times2$ sc supercells (40 atoms) are also presented for comparison. Figure 2 shows the supercells used here.

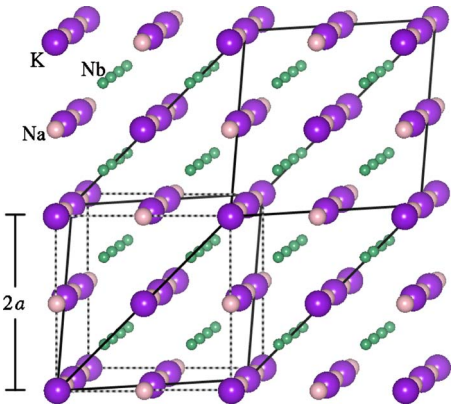

FIG. 2. (Color online) Sc $2\times2\times2$ (40 atoms, dashed line) and fcc $2\times2\times2$ (80 atoms, solid line) supercell of KNN with a rocksaltlike ordering of K and Na. a is the cubic lattice parameter, cf. Table II. Oxygen atoms are omitted for clarity.

The cubic high-temperature structure of KNN 50:50 (the Curie temperature is close to 400 °C) and an ordered solid solution with the K and Na sublattices forming a rocksaltlike structure were assumed throughout. The LDA lattice constant of perfect KNN was used for the defective supercells.

Optimally smooth norm-conserving pseudopotentials as proposed by Vanderbilt,[16] the Ceperley-Alder[17] LDA exchange-correlation functional as parametrized by Perdew and Zunger,[18] and Chadi-Cohen[19] k-point meshes that are equivalent to an $8\times8\times8$ k-point mesh for the simple cubic $1\times1\times1$ unit cell with Gaussian broadening[20] of 0.2 eV were applied. The calculations were performed with the mixed-basis pseudopotential method,[21–25] employing a basis of plane waves up to a maximum energy of 340 eV combined with atom-centered basis functions for alkali $s+p$ semicore states, oxygen p valence states, Nb $s+p$ semicore and d valence states, and Cu d valence states. The atomic positions were relaxed until the maximum force was smaller than 10 meV/Å.

The total energy of the oxygen molecule was calculated in a periodic cubic supercell with an edge length of about 30 Å. The binding energy of the oxygen molecule and the formation enthalpies of the metals were obtained as the total-energy differences compared to single atoms in the same cubic supercell as the O_2 molecule. For the single atoms and the oxygen molecule, spin polarization was taken into account.

Spin polarization of the substitutional Cu impurities was taken into account when calculating the defect-formation energies with the larger (80 atoms) supercells. In the calculations with the smaller supercells (40 atoms), spin polarization was neglected. Test calculations including spin polarization yielded energy differences of about 0.2 eV between the polarized and the unpolarized state, thus the spin polarization of the Cu defects has only a small effect on the defect-formation energies.

TABLE II. Calculated and experimental values for the lattice constants a in Å and the formation energies ΔH_f^0 in eV per formula unit for KNN, its elemental and oxidic reservoirs. The structures of Nb_2O_5, CuO, and A_2O_2 were optimized with respect to volume and internal coordinates. In the case of O_2, a denotes the dimer bond length.

	a calc. in this work	Calc. by others	Expt.	ΔH_f^0 calc. in this work	Calc. by others	Expt.
$KNbO_3$	3.943	3.954 (Ref. 33)	4.00 (Ref. 34)	−14.296		
$NaNbO_3$	3.904	3.914 (Ref. 33)	3.87 (Ref. 34)	−13.852		−13.600 (Ref. 35)
$K_{0.5}Na_{0.5}NbO_3$	3.924		3.94 (Ref. 36)	−14.067		
K (bcc)	4.984	5.09 (Ref. 37)	5.225 (Ref. 38)	−0.963	−1.06 (Ref. 39)	−0.94 (Ref. 39)
Na (bcc)	4.049	4.05 (Ref. 37)	4.224 (Ref. 40)	−1.309	−1.21 (Ref. 41)	−1.113 (Ref. 42)
Nb (bcc)	3.231	3.27 (Ref. 43)	3.303 (Ref. 44)	−8.551	−8.15 (Ref. 43)	−7.57 (Ref. 43)
Cu (fcc)	3.538	3.56 (Ref. 45)	3.61 (Ref. 46)	−4.423	−4.72 (Ref. 39)	−3.49 (Ref. 42)
K_2O	6.176		6.44 (Ref. 47)	−3.792		−3.764 (Ref. 48)
K_2O_2	6.529		6.733 (Ref. 49)	−5.120		−5.139 (Ref. 48)
Na_2O	5.407		5.55 (Ref. 47)	−4.214		−4.299 (Ref. 50)
Na_2O_2	6.146		6.22 (Ref. 51)	−4.687		−5.319 (Ref. 48)
NbO	4.148		4.210 (Ref. 52)	−4.666		−4.206 (Ref. 53)
NbO_2	4.792		4.846 (Ref. 54)	−8.555		−8.239 (Ref. 48)
Z-Nb_2O_5	5.278		5.219 (Ref. 55)	−18.124		−19.687 [a] (Ref. 35)
B-Nb_2O_5	12.600		12.73 (Ref. 56)	−20.805		
CuO	4.631		4.684 (Ref. 57)	−1.440		−1.64 (Ref. 58)
Cu_2O	4.191		4.269 (Ref. 59)	−1.372		−1.75 (Ref. 58)
O_2	1.220	1.22 (Ref. 60)	1.21 (Ref. 60)	−7.467	−7.54 (Ref. 60)	−5.2 (Ref. 60)

[a]Unknown structure modification.

In the case of charged defects a compensating homogeneous background charge density was included in the calculations of electrostatic energies and potentials. The LDA band gap of bulk KNN obtained with a band-structure calculation is about 1.7 eV whereas the experimental band gap of $KNbO_3$ is about 3.3 eV.[26] Because this serious underestimation of the band gap by LDA can affect the gap states and thus the defect-formation energies, we corrected for the LDA band gap by rigidly shifting the conduction-band states upwards by the difference between the experimental and the LDA band gap. For details of this method, see, e.g., Ref. 27. We chose this rather crude method, because there is no preferential first-principles method to correct for LDA band gap errors, which is computationally efficient enough to be applicable to rather large defect supercells. Two potentially applicable approaches are LDA+U (see, e.g., Refs. 28–30) or self-interaction corrected LDA (see, e.g., Refs. 31 and 32). But an application to the KNN system was postponed to a future work. In the graphs showing electronic densities of states, the conduction-band levels were shifted by the band-gap correction as well.

IV. RESULTS

A. Lattice parameters and cohesive energies

In order to validate the computational settings of the mixed basis and the pseudopotentials, the equilibrium lattice parameters and the formation enthalpies with respect to the elements (i.e., the formation energies in the calculations) of KNO, NNO, KNN 50:50, and the elementary and binary reference materials were determined. The results are compared to DFT and experimental data from the literature in Table II.

The lattice constants determined by LDA are systematically underestimated with respect to experimental data in this work as well as in the literature. The cited DFT results of other authors were obtained with the LDA as well. Our results for the lattice constants deviate from the experimental data by less than 3% except for metallic sodium and potassium (4% and 5% deviation, cf. Ref. 37). Some of the formation energies of the metals and the oxides, such as bcc Na, show larger deviations from experiment than the results from literature, others are closer to experiment, such as fcc copper or the oxygen molecule. Altogether, all these deviations from experiment are within the typical range for LDA results and indicate a proper computational setup for the following investigations of point defects.

B. Defect-formation energies of vacancies and substitutional copper atoms in KNN

For the calculation of the defect-formation energies of vacancies and substitutional Cu atoms in KNN the chemical potentials for the points 1–8 in Fig. 1 were determined using Eq. (1). The chemical conditions at each point and the values of the chemical potentials are compiled in Table III. The points 1–3 correspond to an oxygen-rich atmosphere, the points 4–8 to an oxygen-poor one. Since the relative stability of the substitutional defect sites is not affected by the choice of the chemical potential of Cu, the Cu reservoir was always assumed to be metallic ($\Delta\mu_{Cu}=0$).

TABLE III. Chemical potentials in eV for the points 1–8 in the phase stability diagram in Fig. 1.

Point	$\Delta\mu_A$	$\Delta\mu_{Nb}$	$\Delta\mu_O$	Equilibrium between
1	−1.551	−9.815	−0.9001	A_2O_2, A_2O, $ANbO_3$
2	−2.452	−11.615	0.000	O_2, A_2O_2, $ANbO_3$
3	−3.664	−10.402	0.000	O_2, Nb_2O_5, $ANbO_3$
4	−1.817	−1.165	−3.695	Nb_2O_5, NbO_2, $ANbO_3$
5	−1.623	−0.777	−3.889	NbO_2, NbO, $ANbO_3$
6	−0.069	0.000	−4.666	NbO, Nb, $ANbO_3$
7	0.000	0.000	−4.689	A, Nb, $ANbO_3$
8	0.000	−2.058	−4.003	A, A_2O, $ANbO_3$

For the points 1 and 4 in Fig. 1, the defect formation energies of substitutional Cu atoms as function of the Fermi energy are shown in Fig. 3. The Fermi energy is allowed to vary within the range of the experimental band gap (indicated by vertical lines) of 3.3 eV. The regions directly below the VBM and above the conduction-band minimum (CBM) are included in the graphs so that charge transition levels[8] near the band edges are visible since the positions of the charge transition levels may not yet be completely converged with respect to the supercell size. The top of the LDA band gap is also marked by a vertical line [CBM (LDA) in Figs. 3 and 5] but in the following we always refer to the experimental band gap or CBM [CBM (Exp.) in Figs. 3 and 5].

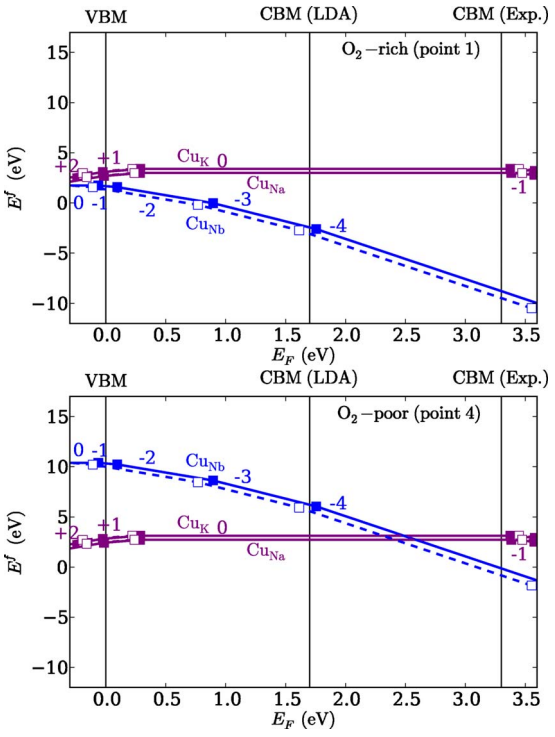

FIG. 3. (Color online) Defect formation energies of substitutional Cu atoms on K, Na, and Nb sites for oxygen-rich conditions (point 1, top) and oxygen-poor ones (point 4, bottom). Squares indicate the charge transition levels. Solid lines and filled squares: fcc 80-atoms supercells, and dashed lines and open squares: sc 40-atoms supercells.

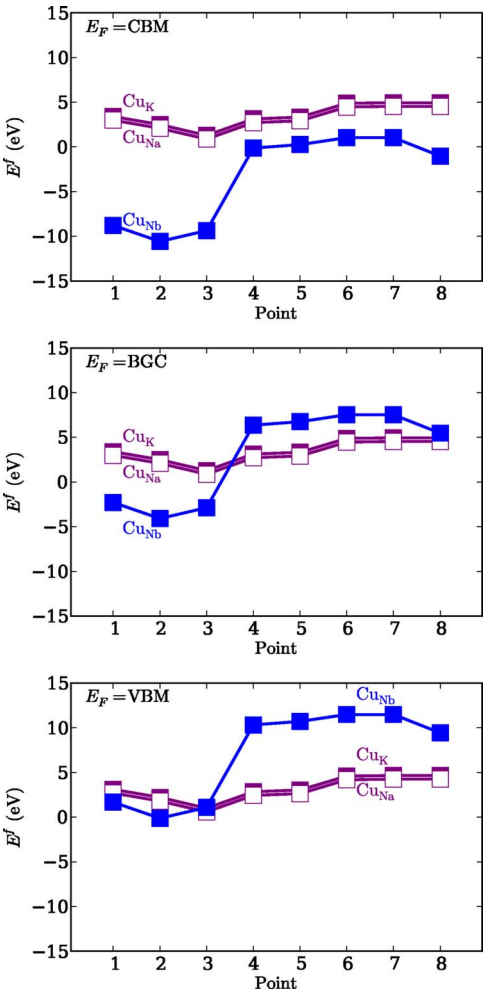

FIG. 4. (Color online) Defect formation energies of Cu dopants on K, Na, and Nb sites in their most stable charge states for the points 1–8, for an electronic chemical potential at the VBM (top), the center of the band gap (BGC, center) and the CBM (bottom).

In an oxygen-rich environment (Fig. 3, top), the Nb sites are energetically favored for Cu substitutionals compared to the alkali sites for Fermi energies in the entire range of the band gap. In a reducing atmosphere (Fig. 3, bottom) the substitution on an alkali site is favorable for Fermi energies in the largest part of the band gap, the Na site being 0.4 eV lower in energy than the K site for equal chemical potentials of K and Na [Eq. (6)].

For most Fermi energies in the band gap, the most stable charge states for substitutional Cu atoms are $q=0$ for Cu on an alkali site and $q=-2$, $q=-3$, or $q=-4$ for Cu on a Nb site, corresponding to Cu^+ on a K^+ or Na^+ site and to Cu^{3+}, Cu^{2+}, or Cu^+ on a Nb^{5+} site (in Kröger-Vink notation; $Cu_A^{\times}$ and Cu''_{Nb}, Cu'''_{Nb}, or Cu''''_{Nb}, respectively).

Whether an alkali site or an Nb site is the energetically preferred lattice site for substitutional Cu atoms hence depends on the chemical potentials and the Fermi level. Figure 4 shows, for which chemical conditions Cu preferentially occupies which lattice site. In the oxygen-rich region (points 1–3), Cu preferentially substitutes for Nb for Fermi energies in the range of the entire band gap (except for point 3, where for a Fermi level at the VBM the two sites are energetically

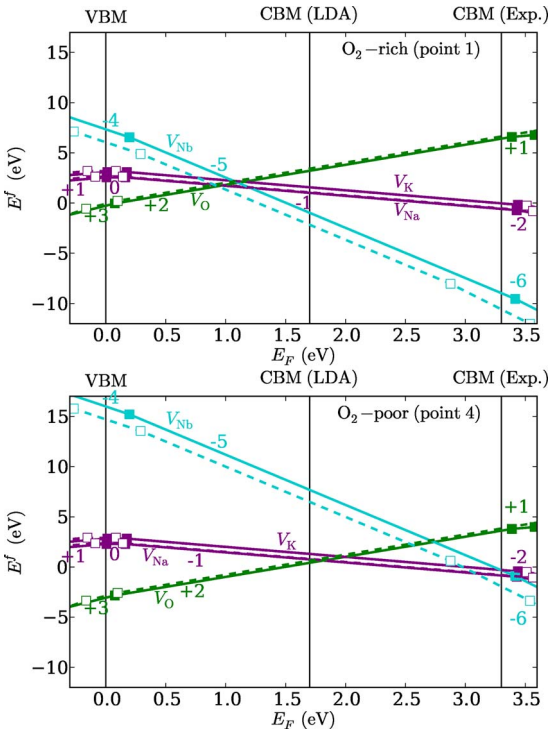

FIG. 5. (Color online) The same as in Fig. 3 for K, Na, Nb, and O vacancies.

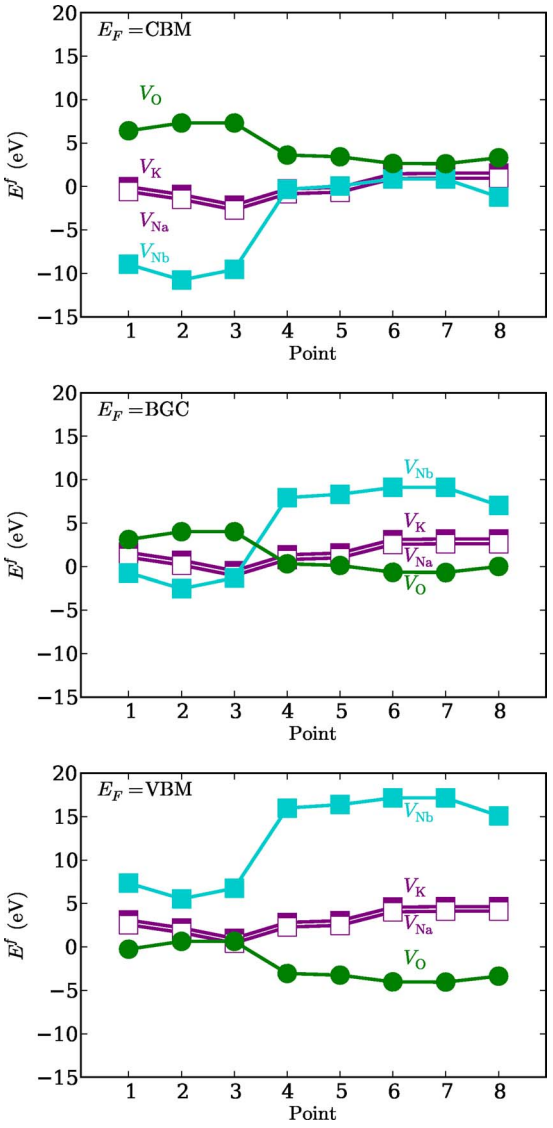

FIG. 6. (Color online) The same as in Fig. 4 for K, Na, Nb, and O vacancies.

degenerated), in a reducing atmosphere (points 4–8), the substitution on an alkali site is energetically more favorable, if the Fermi level lies in the lower half of the band gap or slightly above the center of the band gap.

In Fig. 5, the defect-formation energies of vacancies are shown. In an oxygen-rich atmosphere (Fig. 5, top), oxygen and alkali vacancies prevail for a Fermi energy close to the VBM, whereas Nb vacancies are most favorable for a Fermi energy close to the CBM. In a reducing atmosphere (point 4), oxygen vacancies are most favorable over the entire band-gap range (Fig. 5, bottom). The vacancies are most stable in their nominal charge states V_A^-, V_O^{2+}, and V_{Nb}^{5-} (in Köger-Vink notation; V_A', $V_O^{\bullet\bullet}$, and V_{Nb}''''', respectively). For equal chemical potentials of K and Na, Na vacancies are 0.5 eV lower in energy than K vacancies.

Figure 6 shows the defect-formation energies of K, Na, Nb, and O vacancies in their most stable charge states for a Fermi energy at the VBM (top), the center of the band gap (BGC, center) and at the CBM (bottom), respectively. In agreement with results in Ref. 13, we found that oxygen vacancies prevail in a reducing atmosphere (points 4–8), for a Fermi energy in the lower half of the band gap. But for an oxygen-rich environment (e.g., in air at ambient pressure and temperature) and a Fermi level in the upper half of the band gap or slightly below the band gap center, cation vacancies, especially V_{Nb}, are the most easily formed vacancy types.

The convergence of the defect-formation energies with respect to the supercell size is already good for substitutional Cu atoms on alkali sites and for alkali and oxygen vacancies (at most about 0.24 eV energy difference between the small and the large supercells), and thus a 40-atoms supercell is sufficient to model these defects. When the Nb site is involved, as for substitutional Cu atoms on Nb sites and for Nb vacancies, comparing the 40-atoms cell with the 80-atoms cell shows that the results from the 40-atoms cell are not yet well converged (up to about 1.35 eV energy difference between small and large supercells).

C. Atomic displacements and electronic densities of states in KNN with Cu substitutionals or vacancies

Table IV lists the displacements of the atoms of each species nearest to the Cu substitutional in percent of the equilibrium lattice constant of KNN. For each defect configuration, the charge state which is stable close to the band-gap center was chosen. For Cu on an alkali site, the nearest O and Nb atoms, and for Cu_{Na} also the nearest K atoms, move toward the defect. This can be explained by Cu having a smaller ionic radius than both alkali elements. On the K site this effect is stronger, corresponding to the larger ionic radius of K as compared to Na. The ionic radii (K^+: 1.78 Å, Na^+:

TABLE IV. Displacements, i.e., changes in distance to the defect sites as compared to the ideal structure, of neighbor atoms surrounding the substitutional Cu atom in the sc 40-atoms and fcc 80-atoms $2\times2\times2$ supercells of $K_{0.5}Na_{0.5}NbO_3$ (in percent of the cubic lattice constant a). Positive values indicate displacements away from the defect.

	Cu_K, $q=0$		Cu_{Na}, $q=0$		Cu_{Nb}, $q=-3$	
	40 at.	80 at.	40 at.	80 at.	40 at.	80 at.
K	0.0	0.0	0.0	−0.1	−2.1	−1.3
Na	0.0	0.0	0.0	0.0	−11.6	−9.4
Nb	−0.3	−0.3	−0.1	−0.1	0.0	−1.5
O	−0.6	−0.5	−0.1	−0.1	1.7	1.5

1.53 Å, $Cu^{+}_{K/Na}$: 1.35 Å, and Cu^{2+}_{Nb}: 0.87 Å) were taken from Ref. 61, we extrapolated the one for 12-fold coordinated $Cu^{+}_{K/Na}$ from those for lower coordination numbers.

For Cu on a Nb site, the nearest oxygen ions move away from the defect due to the smaller electrostatic Coulomb attraction caused by the Cu^{2+} ion as compared to the Nb^{5+} ion. The nearest cations move toward the negatively charged defect.

For Cu on an alkali site, the atomic displacements obtained in a 40-atoms supercell are already close to the results from an 80-atoms supercell. But for Cu on an Nb site, the displacements obtained with the two supercell sizes differ considerably. Especially the displacements of the Nb atoms cannot be obtained in a 40-atoms supercell, because if a Cu atom occupies an Nb site, these are zero for symmetry reasons.

Table V shows the displacements of the atoms of each species nearest to a K, Na, Nb, or O vacancy in the 80-atoms $2\times2\times2$ fcc supercell in the charge state with the largest stability range in the LDA band gap. An alkali vacancy, $V^{-}_{K/Na}$, causes the nearest Nb^{5+} ions to move toward the vacancy, whereas the nearest O^{2-} ion moves away from it, as could be expected due to Coulomb attraction and repulsion, respectively. In the case of a K vacancy, the nearest Na^{+} ions move away from the V^{-}_{Ka} defect as well, possibly because they are attracted by the oxygen ions or repelled by the niobium ions. An Nb vacancy V^{5-}_{Nb} attracts the nearest cations and repels the oxygen ions whereas an oxygen vacancy, V^{2+}_{O}, repels the nearest cations and attracts the nearest oxygen ions due to Coulomb interaction.

Figures 7–9 show electronic densities of states (DOS) for perfect KNN, for KNN with a Cu dopant on a K or Nb site, and for KNN with K, Na, Nb, or O vacancies. The VBM of the perfect and the defective crystals are set to zero. The shaded areas beneath the curves indicate occupied energy levels. In the DOS, the energy for which the DOS of the pure material changes from zero to a finite number was taken as the VBM and the CBM was set to $E_{VBM}+E_G$ with E_G being the experimental band gap. The defective DOS was aligned with the perfect one in such a way that certain VBM and CBM features, which are present in the DOS of both the perfect and the defective KNN, lie at the same energy. The conduction band levels were shifted upward by the difference between LDA and experimental conduction band. The Cu d levels were assigned to the valence band and were not shifted. The VBM, the LDA [CBM (LDA)] and the experimental CBM [CBM (Exp.)] are indicated by vertical lines. The differences in number of spin-up and spin-down electrons $\Delta n_{\uparrow\downarrow}$ for each defect and charge state are listed in Table VI.

TABLE V. The same as in Table IV, for K, Na, Nb, and O vacancies.

	V_K, $q=-1$	V_{Na}, $q=-1$	V_{Nb}, $q=-5$	V_O, $q=+2$
K	0.0	0.0	−3.1	1.6
Na	0.8	0.0	−18.6	2.8
Nb	−0.9	−0.6	−1.3	4.2
O	0.8	1.5	3.1	−4.0

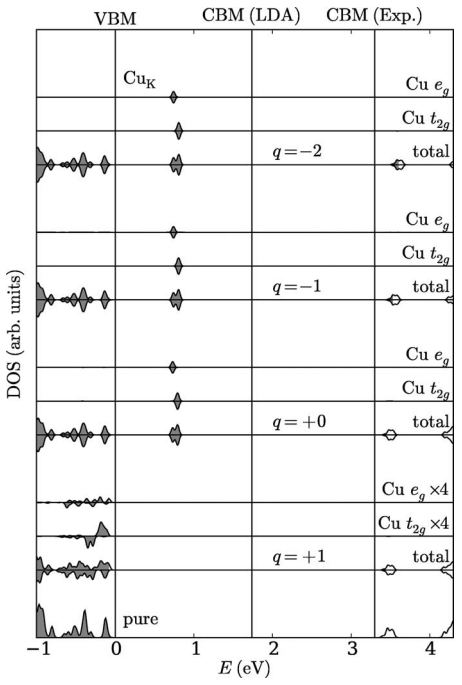

FIG. 7. Total and partial (Cu d) electronic DOS for pure KNN and for KNN with substitutional Cu atoms on K sites in their stable charge states. The VBM is set to zero, the VBM and the CBM are indicated by vertical lines. For the two curves $q=+1$ the partial DOS are scaled by a factor of 4 for better visibility.

TABLE VI. Differences in numbers of spin-up and spin-down electrons $\Delta n_{\uparrow\downarrow}$ of Cu substitutionals on alkali and Nb sites for different charge states q.

	$Cu_{K/Na}$				Cu_{Nb}			
q	+1	0	−1	−2	−1	−2	−3	−4
$\Delta n_{\uparrow\downarrow}$	1	0	0	0	3	2	1	0

For Cu on the two alkali sites (Fig. 7), almost identical densities of states are obtained, so we show only the one for Cu on a K site. In the charge state $q=+1$, stable for a Fermi energy close to the VBM, the Cu substitutional generates a hole in the VBM (cf. Table VII). There are no gap levels. The Cu atom is spin polarized (cf. Table VI). In the charge state $q=0$, which is stable for Fermi energies over the most part of the band gap, Cu on an alkali site introduces gap states approximately 0.8 eV above the VBM, which consist of Cu e_g and t_{2g} states. These gap states are fully occupied by electrons and the Cu impurity is unpolarized. If more electrons are added, they occupy the conduction band without modifying the defect levels.

For Cu on a Nb site (Fig. 8), for all charge states that are stable for a Fermi energy in the band gap, gap states are present and the Cu atom is spin polarized for all Fermi levels in the lower half of the band gap. In the charge state $q=-1$, which is the most stable charge state for a Fermi energy in a range of 0.3 eV above the VBM, the Cu substitutional generates a hole in the valence band. The Cu e_g states are split by spin polarization. Two e_g levels lie inside the valence band, the other two are unoccupied and lie about 0.6 eV above the VBM. In the charge state $q=-2$, the valence band is completely occupied by electrons, the gap states are unoccupied. For $q=-3$, which is stable near the center of the band gap, all the Cu e_g states have shifted into the band gap. Two levels are situated about 0.7 eV above the VBM and are completely occupied, the other two lie about 1.3 eV above the VBM and are half occupied. In the charge state $q=-4$, which is stable in the upper part of the band gap, one of the defect levels has moved upward and is now situated close to the band-gap center. All defect levels are now fully occupied by electrons and the Cu atom is unpolarized.

In the charge states that are stable over the most part of the band gap, the K, Na (again omitted because of strong similarity to K), Nb, and O vacancies generate neither holes in the valence band nor free electrons in the conduction band (cf. Fig. 9 and Table VIII). However, for a Fermi energy close to the VBM, each vacancy type generates a hole in the valence band. For charge states that are stable slightly above the CBM, all vacancy types lead to electrons in the conduction band.

V. DISCUSSION

In Ref. 62 Zhang relates the Fermi energies, at which p-type and n-type defects have zero formation energy, to the minimum and maximum possible Fermi energy (pinning energies). For example, negative defect-formation energies for

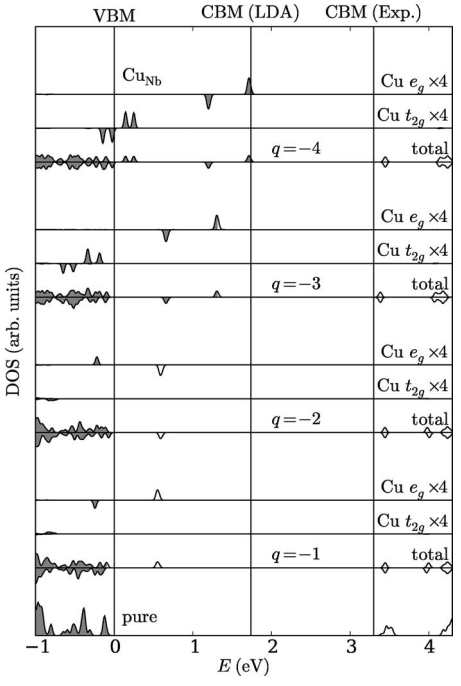

FIG. 8. The same as in Fig. 7 for Cu atoms on Nb sites. The Cu d DOS is scaled by a factor of 4 for better visibility.

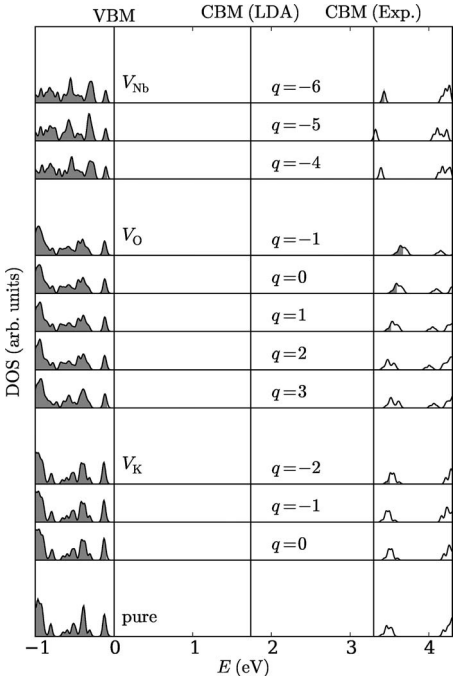

FIG. 9. The same as in Fig. 7 for K, Nb, and O vacancies.

TABLE VII. Number of holes in the valence band (n_h) and of electrons in the conduction band (n_e) for substitutional Cu defects in different charge states q.

	$Cu_{K/Na}$				Cu_{Nb}			
q	+1	0	−1	−2	−1	−2	−3	−4
n_h	1	0	0	0	1	0	0	0
n_e	0	0	1	2	0	0	0	0

V_O in a reducing atmosphere and for Fermi energies in the lower half of the band gap indicate that O_2 gazes out and the Fermi level increases until it reaches the range where the defect-formation energies are positive. For vacancies, we obtained negative formation energies of p-type defects near the VBM and of n-type ones near the CBM so that the Fermi energy should be pinned to a region around the center of the band gap (BGC). In the following discussion of defect formation energies, we therefore assume that the Fermi level lies close to the BGC. However, the boundaries of this stability region depend on the atomic chemical potentials, e.g., via the oxygen partial pressure.

Our results show that the temperature and the oxygen partial pressure determine the preferred substitution site for Cu in KNN. In air at ambient pressure and temperature Cu is energetically driven to substitute on Nb sites, but for temperatures around 1300 K and reduced O_2 pressures (μbar or lower), the substitution on the alkali sites becomes more favorable. Our results indicate that an Nb substitution is rather more favorable for typical processing conditions (in air at temperatures up to about 1300 K), but the alkali substitution cannot be ruled out completely. K_2O is quite volatile and tends to gaze out to some extent, which can lead to K vacancies. The vacant K sites might then be occupied by Cu, which could explain why in Ref. 7 evidence was found for Cu substituting on A sites for small Cu concentrations. Recent experimental studies using electron paramagnetic resonance (EPR) spectroscopy[63] found evidence for Cu substituting for Nb. Since we found that in their most stable charge states, the Cu_{Nb} defects are spin-polarized for most Fermi energies in the band gap, whereas the $Cu_{K/Na}$ defects are unpolarized, the latter may not be detected by EPR spectroscopy. The negative defect-formation energies for some conditions are due to our choice of metallic Cu as reservoir (the absolute number of μ_{Cu} is not needed here because we are interested in the relative stability of $Cu_{K/Na}$ as compared to Cu_{Nb}) and do not indicate instability of the host perovskite with respect to exchange of, e.g., Nb for Cu.

The Cu impurities mainly occur in the charge states $Cu_A^{\times}$ and Cu_{Nb}'''/Cu_{Nb}'''', although $Cu_A^{\bullet}$ and Cu_{Nb}'' are also stable over a certain energy range in the lower part of the band gap. The charge transition levels between $q=-2$ and $q=-3$ and between $q=-3$ and $q=-4$ of the Cu_{Nb} defect are located slightly below the center of the LDA band gap and slightly above the LDA CBM (which is located about 1.7 eV above the VBM), respectively, analogous to the transitions between $q=-1$ and $q=-2$ and between $q=-2$ and $q=-3$ found for Cu_{Ti} in PTO.[11]

In Ref. 11, Erhart *et al.* reported the differences in spin-up and spin-down electrons $\Delta n_{\uparrow\downarrow}$ for Cu_{Ti}' ($\Delta n_{\uparrow\downarrow}=2$) and Cu_{Ti}''($\Delta n_{\uparrow\downarrow}=1$) in PTO. For the corresponding charge states of Cu on Nb sites in KNN (Cu_{Nb}'' and Cu_{Nb}'''), we found the same differences in spin-up and spin-down electrons, $\Delta n_{\uparrow\downarrow}=2$ for Cu_{Nb}'' and $\Delta n_{\uparrow\downarrow}=1$ for Cu_{Nb}'''. However, for determining defect-formation energies, the effect of the spin polarization is rather small. An unpolarized calculation is already sufficient for obtaining the relative stability of the possible lattice sites and the approximate positions of the charge transition levels for Cu substitutionals in KNN.

Cu on an alkali site is an uncharged impurity for most Fermi energies inside the band gap and the atomic displacements are rather small in this case (0.6% of a at most). Therefore neither electrostatic nor elastic interactions are large or long-ranged so that already rather small supercells containing 40 atoms apparently are sufficient to model these defects. The same holds for alkali and oxygen vacancies even though the latter defects are charged.

If Cu occupies a Nb site, the atomic displacements (up to 11.6% of a) and the defect charges are large, and a 40-atoms supercell does not yet yield well-converged results. This is only partly due to the symmetry of the sc $2\times2\times2$ supercell, which prevents displacements of the Nb ions toward or away from the impurity in the case of Cu_{Nb}. A band-structure calculation (not shown) for the smaller supercell (40 atoms) shows that the Cu e_g states still show a considerable dispersion, which is pretty much reduced in the 80-atoms supercell, in accordance with results from Ref. 14 for Fe impurities in $KNbO_3$.

The displacements of the atoms nearest to a Cu substitutional or a vacancy can mostly be explained in terms of Cou-

TABLE VIII. The same as in Table VII for vacancies.

	$V_{K/Na}$			V_{Nb}			V_O				
q	0	−1	−2	−4	−5	−6	+3	+2	+1	0	−1
n_h	1	0	0	1	0	0	1	0	0	0	0
n_e	0	0	1	0	0	0	0	0	1	2	3

lomb interaction between ions and charged defects, i.e., negatively charged defects attract the nearest cations and repulse the nearest anions, and vice versa for positively charged defects. The atomic displacements near to a vacancy are in qualitative and for the cations also in quantitative agreement with results presented in Ref. 13 for vacancies in $KNbO_3$.

In a reducing atmosphere, oxygen vacancies are the prevailing vacancy type, also alkali vacancies form easily. If the oxygen partial pressure is on the order of the standard atmospheric pressure, cation vacancies, especially V_{Nb}, become energetically more favorable.

Over the most part of the band gap, the vacancies are most stable in their nominal charge states $V'_{K,Na}$, V''''_{Nb}, and $V^{\bullet\bullet}_{O}$, and thus do not generate free charge carriers. In the defect charge states of vacancies and Cu substitutionals that are stable over the most part of the band gap, the valence band is completely occupied, and the substitutional Cu atoms introduce deep levels. Thus, in this case it is unlikely that free charge carriers are generated and the electronic conductivity of the material should hardly be enhanced by either the Cu substitutionals or the vacancies. However, for a Fermi energy in a range of about 0.3 eV above the VBM, charge transition levels were found for all types of defects considered here, Cu substitutionals and vacancies, and the defects generate holes in the valence band. For the charge states which become stable for Fermi energies slightly above the CBM, electrons occupy the conduction band, so that Cu dopants and vacancies would increase the number of free electrons in the material.

Since we found empty or partly filled deep levels for Cu on Nb sites for a Fermi energy over the most part of the band gap, the Cu_{Nb} defect likely acts as a trap for electrons. Trapping of charge carriers at impurities is assumed to play a role in electrical fatigue of ferroelectrics.[64]

VI. SUMMARY

In a strongly reducing atmosphere, the preferred lattice site for substitional Cu is the Na or K site, and the prevailing vacancy type is the oxygen vacancy. In an oxygen-rich environment the Nb site is more stable for substitutional Cu atoms, and the most common vacancies are Nb and possibly alkali vacancies. Cu substitutionals on Nb sites were found to occur mainly in the charge states Cu''_{Nb}, Cu'''_{Nb}, and Cu''''_{Nb}, on an alkali site $Cu^{\times}_{K,Na}$ is most stable for a Fermi energy in the largest part of the band gap. The vacancies are most stable in their nominal ionic charge states $V'_{K/Na}$, V''''_{Nb}, and $V^{\bullet\bullet}_{O}$, respectively. Neither vacancies nor Cu dopants in their stable charge states should lead to free charge carriers in the material, except for a Fermi energy close to the band edges. We found that Cu substitutionals on Nb sites are spin-polarized for a Fermi energy close to the center of the band gap whereas on the alkali sites they are unpolarized.

ACKNOWLEDGMENTS

This work was funded by the German Research Foundation (Project No. EL 155/21-1). The authors gratefully acknowledge helpful discussions with A. T. Paxton, R.-A. Eichel, H. Kungl, and M. J. Hoffmann. The perovskite structure was visualized with VESTA (Ref. 65).

*sabine.koerbel@iwm.fraunhofer.de

[1] Y. Saito, H. Takao, T. Tani, T. Nonoyama, K. Takatori, T. Homma, T. Nagaya, and M. Nakamura, Nature (London) **432**, 84 (2004).
[2] J. Acker, H. Kungl, and M. J. Hoffmann, J. Am. Ceram. Soc. **93**, 1270 (2010).
[3] M. Matsubara, T. Yamaguchi, K. Kikuta, and S. Hirano, Jpn. J. Appl. Phys., Part 1 **43**, 7159 (2004).
[4] M. Matsubara, T. Yamaguchi, W. Sakamoto, K. Kikuta, T. Yogo, and S. Hirano, J. Am. Ceram. Soc. **88**, 1190 (2005).
[5] J. Svoboda, H. Riedel, and R. Gaebel, Acta Mater. **44**, 3215 (1996).
[6] R. Zuo, C. Ye, X. Fang, Z. Yue, and L. Li, J. Am. Ceram. Soc. **91**, 914 (2008).
[7] E. Li, H. Kakemoto, S. Wada, and T. Tsurumi, J. Am. Ceram. Soc. **90**, 1787 (2007).
[8] C. Van de Walle and J. Neugebauer, J. Appl. Phys. **95**, 3851 (2004).
[9] K. Reuter and M. Scheffler, Phys. Rev. B **65**, 035406 (2001).
[10] P. Erhart and K. Albe, J. Appl. Phys. **102**, 084111 (2007).
[11] P. Erhart, R.-A. Eichel, P. Träskelin, and K. Albe, Phys. Rev. B **76**, 174116 (2007).
[12] A. Shigemi and T. Wada, Jpn. J. Appl. Phys., Part 1 **43**, 6793 (2004).
[13] A. Shigemi and T. Wada, Jpn. J. Appl. Phys., Part 1 **44**, 8048 (2005).
[14] A. V. Postnikov, A. I. Poteryaev, and G. Borstel, Ferroelectrics **206**, 69 (1998).
[15] *CRC Handbook of Chemistry and Physics*, 89th ed., edited by D. R. Lide (CRC, Boca Raton, 2008).
[16] D. Vanderbilt, Phys. Rev. B **32**, 8412 (1985).
[17] D. M. Ceperley and B. J. Alder, Phys. Rev. Lett. **45**, 566 (1980).
[18] J. P. Perdew and A. Zunger, Phys. Rev. B **23**, 5048 (1981).
[19] D. J. Chadi and M. L. Cohen, Phys. Rev. B **8**, 5747 (1973).
[20] C. L. Fu and K. M. Ho, Phys. Rev. B **28**, 5480 (1983).
[21] C. Elsässer, N. Takeuchi, K. M. Ho, C. T. Chan, P. Braun, and M. Fähnle, J. Phys.: Condens. Matter **2**, 4371 (1990).
[22] K. Ho, C. Elsässer, C. Chan, and M. Fähnle, J. Phys.: Condens. Matter **4**, 5189 (1992).
[23] B. Meyer, K. Hummler, C. Elsässer, and M. Fähnle, J. Phys.: Condens. Matter **7**, 9201 (1995).
[24] F. Lechermann, F. Welsch, C. Elsässer, C. Ederer, M. Fähnle, J. M. Sanchez, and B. Meyer, Phys. Rev. B **65**, 132104 (2002).
[25] B. Meyer, F. Lechermann, C. Elsässer, and M. Fähnle, FORTRAN90 Program for Mixed-Basis Pseudopotential Calculations for Crystals, Max-Planck-Institut für Metallforschung, Stuttgart.
[26] E. Wiesendanger, Ferroelectrics **6**, 263 (1974).
[27] A. F. Kohan, G. Ceder, D. Morgan, and Chris G. Van de Walle,

Phys. Rev. B **61**, 15019 (2000).
[28] N. J. Mosey and E. A. Carter, Phys. Rev. B **76**, 155123 (2007).
[29] E. Carter, Science **321**, 800 (2008).
[30] F. Lechermann, M. Fähnle, B. Meyer, and C. Elsässer, Phys. Rev. B **69**, 165116 (2004).
[31] W. Körner and C. Elsässer, Phys. Rev. B **81**, 085324 (2010).
[32] D. Vogel, P. Krüger, and J. Pollmann, Phys. Rev. B **55**, 12836 (1997).
[33] R. D. King-Smith and D. Vanderbilt, Phys. Rev. B **49**, 5828 (1994).
[34] G. Shirane, R. Newnham, and R. Pepinsky, Phys. Rev. **96**, 581 (1954).
[35] I. Pozdnyakova, A. Navrotsky, L. Shilkina, and L. Reznitchenko, J. Am. Ceram. Soc. **85**, 379 (2002).
[36] J. Attia, L. Bellaiche, P. Gemeiner, B. Dkhil, and B. Malic, J. Phys. IV **128**, 55 (2005).
[37] W. Frank, C. Elsässer, and M. Fähnle, Phys. Rev. Lett. **74**, 1791 (1995).
[38] C. S. Barrett, Acta Crystallogr. **9**, 671 (1956).
[39] P. Bagno, O. Jepsen, and O. Gunnarsson, Phys. Rev. B **40**, 1997 (1989).
[40] H. Abe, K. Oshima, T. Suzuki, and Y. Watanabe, J. Appl. Crystallogr. **27**, 1040 (1994).
[41] S. H. Vosko and L. Wilk, Phys. Rev. B **22**, 3812 (1980).
[42] C. Kittel, *Introduction to Solid State Physics*, 7th ed. (Wiley, New York, 1996).
[43] A. García, C. Elsässer, J. Zhu, S. G. Louie, and M. L. Cohen, Phys. Rev. B **46**, 9829 (1992).
[44] M. C. Neuburger, Z. Anorg. Allg. Chem. **197**, 219 (1931).
[45] A. Hashibon, C. Elsässer, Y. Mishin, and P. Gumbsch, Phys. Rev. B **76**, 245434 (2007).
[46] M. Straumanis and L. Yu, Acta Crystallogr., Sect. A: Cryst. Phys., Diffr., Theor. Gen. Crystallogr. **25**, 676 (1969).
[47] R. Dovesi, C. Roetti, C. Freyria-Fava, M. Prencipe, and V. R. Saunders, Chem. Phys. **156**, 11 (1991).
[48] NIST-JANAF Thermochemical Tables, 4th ed., edited by M. W. Chase, Jr., J. Phys. Chem. Ref. Data Monogr. **9** (1998).
[49] T. Bremm and M. Jansen, Z. Anorg. Allg. Chem. **610**, 64 (1992).
[50] P. A. G. O'Hare, J. Chem. Phys. **56**, 4513 (1972).
[51] J. L. Tallman, R. L. Margrave, and S. W. Bailey, J. Am. Chem. Soc. **79**, 2979 (1957).
[52] A. Bowman, T. Wallace, J. Yarnell, and R. Wenzel, Acta Crystallogr. **21**, 843 (1966).
[53] H. Schäfer and F. Liedmeier, Z. Anorg. Allg. Chem. **329**, 225 (1964).
[54] A. A. Bolzan, C. Fong, B. J. Kennedy, and C. J. Howard, Acta Crystallogr., Sect. B: Struct. Sci. **53**, 373 (1997).
[55] I. Zibrov, V. Filonenko, P.-E. Werner, B.-O. Marinder, and M. Sundberg, J. Solid State Chem. **141**, 205 (1998).
[56] F. Laves, W. Petter, and H. Wulf, Naturwiss. **51**, 633 (1964).
[57] S. Åsbrink and L.-J. Norrby, Acta Crystallogr., Sect. B: Struct. Crystallogr. Cryst. Chem. **26**, 8 (1970).
[58] *CRC Handbook of Chemistry and Physics*, 64th ed., edited by R. C. Weast (CRC Press, Boca Raton, 1984).
[59] A. Kirfel and K. Eichhorn, Acta Crystallogr., Sect. A: Found. Crystallogr. **46**, 271 (1990).
[60] G. S. Painter and F. W. Averill, Phys. Rev. B **26**, 1781 (1982).
[61] R. Shannon, Acta Crystallogr., Sect. A: Cryst. Phys., Diffr., Theor. Gen. Crystallogr. **32**, 751 (1976).
[62] S. B. Zhang, J. Phys.: Condens. Matter **14**, R881 (2002).
[63] R. Eichel, E. Erünal, M. Drahus, D. Smyth, J. Tol, J. Acker, H. Kungl, and M. Hoffmann, Phys. Chem. Chem. Phys. **11**, 8698 (2009).
[64] W. L. Warren, D. Dimos, B. A. Tuttle, G. E. Pike, and H. N. Al-shareef, Integr. Ferroelectr. **16**, 77 (1997).
[65] K. Momma and F. Izumi, J. Appl. Crystallogr. **41**, 653 (2008).